arXiv:0806.4226v2 [astro-ph] 27 Jun 2008

Resolving a Class I Protostar Binary System with Chandra

Kenji Hamaguchi[1,2], Minho Choi[3], Michael F. Corcoran[1,4], Chul-Sung Choi[3], Ken'ichi Tatematsu[5], Rob Petre[6]

ABSTRACT

Using a sub-pixel event repositioning technique, we spatially resolved X-ray emission from the infrared double system IRS 5 in the R Corona Australis molecular cloud with $\sim 0.''8$ separation. As far as we know, this result - obtained from 8 Chandra archival observations between 2000 and 2005 - is the first X-ray study of individual sources in a Class I protostar binary system with a projected separation of less than 200 AU. We extracted light curves and spectra of the individual sources using a two-dimensional image fitting method. IRS 5a at the south, the source which was brighter in the near-infrared, showed three X-ray flares lasting >20 ksec, reminiscent of X-ray flares from pre-main sequence stars, while the northern source (IRS 5b) was quiescent in X-rays in all the observations except for a 2005 August 9 observation with a factor of $\sim$2 flux enhancement. In quiescence, these sources showed almost identical X-ray spectra, with $N_{\rm H}$ $\sim 4\times10^{22}$ cm^{-2}, $kT \sim$2 keV, and log $L_{\rm X} \sim$30.2$-$3 erg s^{-1}. IRS 5a showed plasma at temperatures up to $kT \sim$5$-$6 keV during flares, while the column density of IRS 5b increased by a factor of 2 during an observation on 2005 August 9. We discuss the evolutionary stages and variation of the X-ray activity of these sources.

Subject headings: techniques: high angular resolution — binaries: visual — stars: magnetic fields — stars: pre–main-sequence — X-rays: stars

1. Introduction

Many, if not most, stars are born as a member of a multiple system through fragmentation of the parent molecular cloud. Because young stellar objects (YSOs) that form as a binary or multiple system are of the same age and chemical composition, any differences in the level of their stellar activity should be due to differences of stellar initial parameters such as mass, net angular momentum and/or the presence of the companion star (See reviews about multiplicity of young stars in Duchêne et al. 2007; Monin et al. 2007, and magnetic activity on various stellar parameters in ex. Chabrier & Küker 2006; Dobler et al. 2006). YSO binaries are therefore a useful probe to test models of the dependence of the activity on stellar parameters for stars of the same age.

The R Corona Australis (R CrA) molecular cloud has rich association of YSOs with various evolutionary stages (Taylor & Storey 1984). Among them, IRS 5 (a.k.a. TS 2.4) suffers strong extinction ($A_{\rm V}$ $\sim$45 mag) and is classified as a Class I protostar (Wilking et al. 1986, 1992, see therein for the spectral classification of YSOs). High angular resolution near-infrared imaging separated IRS 5 into two stellar components, IRS 5a (K $\sim 10.9^{m}$) and IRS 5b (K $\sim 11.5^{m}$). The separation of the two stars is less than an arcsecond (Chen & Graham 1993; Nisini et al. 2005). In

---

[1] CRESST and X-ray Astrophysics Laboratory NASA/GSFC, Greenbelt, MD 20771

[2] Department of Physics, University of Maryland, Baltimore County, 1000 Hilltop Circle, Baltimore, MD 21250

[3] International Center for Astrophysics, Korea Astronomy and Space Science Institute, Hwaam 61-1, Yuseong, Daejeon 305-348, South Korea

[4] Universities Space Research Association, 10211 Wincopin Circle, Suite 500, Columbia, MD 21044

[5] National Astronomical Observatory of Japan, 2-21-1 Osawa, Mitaka, Tokyo 181-8588, Japan

[6] Astrophysics Science Division, NASA Goddard Space Flight Center, Greenbelt, MD 20771

`Mail to:` Kenji.Hamaguchi@nasa.gov

what follows the term IRS 5 means the entire binary system, or is used when the emitting source was unknown due to limited imaging capability. The southern source, IRS 5a, has a stellar spectral type of K5-K7V and is located in a low mass protostar phase on the HR diagram (Nisini et al. 2005). Stellar parameters of IRS 5b are poorly known due to its faintness.

IRS 5 is also known as one of the rare Class I protostars showing strongly variable cm continuum radio emission (Suters et al. 1996) with significant circular polarization (Feigelson et al. 1998). Such gyrosynchrotron radio emission is believed to be the major radio emission mechanism of weak-lined T-Tauri Stars (wTTSs, e.g. Carkner et al. 1997), but the emission from protostars is supposed to be absorbed by the surrounding ionized materials heated by mass accretion. IRS 5 does not currently show strong mass accretion activity, but there is evidence of an outflow possibly driven by IRS5 (HH 731, Wang et al. 2004). The near-infrared spectrum of IRS 5a shows small continuum excess above the photospheric flux, which also suggests a low accretion rate (Nisini et al. 2005). The infrared spectrum also shows characteristics of scattered emission. From these results, Nisini et al. (2005) questioned the idea that the IRS 5 system is a bona-fide protostar, but it may be close to the TTS phase.

IRS 5 also showed strongly absorbed thermal X-ray emission ($N_{\rm H}$ $\sim$4$\times$10^{22} cm^{-2}, kT $\sim$2 keV, Koyama et al. 1996; Neuhäuser & Preibisch 1997; Forbrich et al. 2006, 2007; Forbrich & Preibisch 2007). The emission was highly variable, accompanied by occasional rapid flares. These X-ray characteristics are consistent with plasma heating by magnetic activity in the stellar corona, so that the X-ray and radio emission from IRS 5 is suspected to arise from the same root cause. Similarly, Forbrich et al. (2007) did not find a clear correlation between the X-ray and near-infrared flux variation from IRS 5 and other cluster members, which tends to support a coronal origin for the X-ray activity instead of accretion driven activity.

To understand the relation between the X-ray and radio activity of IRS 5 and study the evolution of the activity, we need to resolve the IRS 5 binary system in both wavelengths. Choi et al. (2008) successfully resolved IRS 5 into two cm radio sources in a VLA radio observation. Resolving X-ray sources with a sub-arcsecond separation is challenging even with the *Chandra* observatory with its unprecedented X-ray angular resolution. However, encouraged by a marginal resolution of IRS 5 in a *Chandra* image (see Figure 5 of Forbrich et al. 2007), we revisited *Chandra* archival observations of IRS 5 and clearly resolved the individual binary components using enhanced spatial information obtained with the Sub-pixel Event Repositioning (SER) technique (Tsunemi et al. 2001; Li et al. 2003, 2004). Using this technique we were also able to extract light curves and spectra of each source with a two-dimensional image fitting method and measured the plasma parameters of individual binary stars for the first time.

The distance to the cloud is controversial. Marraco & Rydgren (1981) estimated it to be 129 pc from uvbyβ photometry of three stars in the cloud. Assuming $A_{\rm V}$ =3.1 mag, Casey et al. (1998) derived the same distance (129±11 pc) to the eclipsing binary TY CrA, which is suspected to be a cluster member. However, Knude & Hϕg (1998) measured d = 170 pc from the interstellar reddening of stars in the cloud having *HIPPARCOS* distances and Tycho B - V colors, and whose distance we use for IRS 5.

2. Observations

We found eight archival pointings with *Chandra* (Weisskopf et al. 2002) that include IRS 5 in the FOV (Table 1). These observations occurred between 2000 October and 2005 August and used the Advanced CCD Imaging Spectrometer with the Imaging array (ACIS-I) at the prime focus with exposure times between 15−40 ksec. During the observations, IRS 5 was put at $1'-2'$ off-axis, where the PSF quality is negligibly different from the on-axis position. We use the convention that individual *Chandra* observations are designated CXO, subscripted with the year, month and day of the observation. We downloaded the data from the HEASARC archive[1] and reprocessed them with the CIAO[2] analysis software version 3.4 (CALDB ver. 3.3.0.1). We reprocessed the data, removed

---

[1] http://heasarc.gsfc.nasa.gov/W3Browse/

[2] http://cxc.harvard.edu/ciao/

TABLE 1
JOURNAL OF THE *Chandra* OBSERVATIONS

Abbreviation	Seq. ID	Observation Start	Exposure (ksec)	Image Shift Δ (R.A., Dec.) (arcsec)	Image Shift StdDev (mas)	Off-axis (arcsec)
CXO_{001007}	19	2000 Oct 7 17:02	19.7	(0.40, 0.96)	128	59.3
CXO_{030626}	3499	2003 Jun 26 12:58	37.6	(0.56, 0.28)	81	90.0
CXO_{040617}	4475	2004 Jun 17 23:17	19.9	(0.19, 0.21)	117	114.2
CXO_{050808}	5402	2005 Aug 8 2:38	15.2	(0.07, 0.06)	88	72.1
CXO_{050809}	5403	2005 Aug 9 2:39	15.0	(0.06, 0.11)	109	72.4
CXO_{050810}	5404	2005 Aug 10 1:58	15.0	(0.08, 0.06)	67	72.5
CXO_{050812}	5405	2005 Aug 12 3:13	15.0	(0.06, 0.12)	144	72.5
CXO_{050813}	5406	2005 Aug 13 1:51	14.6	(0.03, 0.01)	189	72.6

NOTE.—Seq. ID: sequence identification number of each observation. Image Shift: shift of the X-ray sky coordinate frame from the original X-ray data to the 2 MASS frame. StdDev: standard offset deviation of the X-ray source positions from the 2MASS source positions in milli-arcsecond. Off-axis: off-axis angle of IRS 5 from the nominal point.

the pixel randomization and utilized the SER algorithms to improve the spatial resolution.

Photon pile-up can cause source count rates to be underestimated, spectral shapes to appear harder, and degrades event position determination in the SER method. Fortunately, observed X-ray photon counts of IRS 5 ranged between 0.02−0.08 counts s^{-1}, corresponding to small pile-up fractions of ∼2−8 %[3]. We thus did not correct for any pile-up effect in our analysis.

3. Analysis and Results

3.1. Absolute Astrometry

This study crucially requires absolute astrometry of the X-ray images with a few tenths of arcsecond precision. We therefore measured sky positions of X-ray sources around IRS 5 and cross-correlated them with sources in the Point Source Catalog of the 2MASS All-Sky Data Release.

There is up to 7 year time span between the interval when the 2MASS observations of the southern sky (1998 March – 2001 February) and the *Chandra* observations (2000 Oct – 2005 Aug). The cluster members can move significantly within 7 years if their proper motions are suitably large. The *HIPPARCOS* catalogue has 4 sources with proper motion measurements (Perryman & ESA 1997). Among them, R CrA and V709 CrA have proper motion of ∼80−100 mas yr^{-1}, but they have large uncertainty in the parallax measurement (∼68, 140 mas) and almost opposite directions in their proper motions. This would suggest that their measurements are less reliable, possibly due to contamination of surrounding nebular emission. Two other sources, TY CrA and HD 176386, with better parallax measurements have small proper motions ($\lesssim$20 mas yr^{-1}). Our tentative measurement of the proper motion of cluster members using VLA data between 1997 and 2005 also derived similarly small proper motions of $\lesssim$28 mas yr^{-1}(Choi et al. 2008). These results suggest that the proper motion of the cluster members is small, less than ∼150 mas in 7 years ($\lesssim$1 pixel in the Figure 1 image).

To measure X-ray source positions in each observation, we ran the *wavdetect* source detection tool in the CIAO package for a 0.35−8 keV image binned at $0.''5$ pixel^{-1} and only considered sources at above the 4σ significance. The 2MASS positions of IRS 1, IRS 2, R CrA, IRS 13 and HBC 667 had corresponding X-ray counterparts with similar offsets ($\lesssim 0.''1$ between the sources, see source positions in Figure 1 of Hamaguchi et al. 2005 and Forbrich et al. 2006), while there was no counterpart to the X-ray source corresponding to IRS 6 in the 2MASS catalogue within $1''$.[4] We therefore used the former 5 sources for the positional references.

The 2MASS positions of IRS 1, IRS 2, R CrA,

---

[3] http://heasarc.gsfc.nasa.gov/Tools/w3pimms.html

[4] It was in the "reject" table.

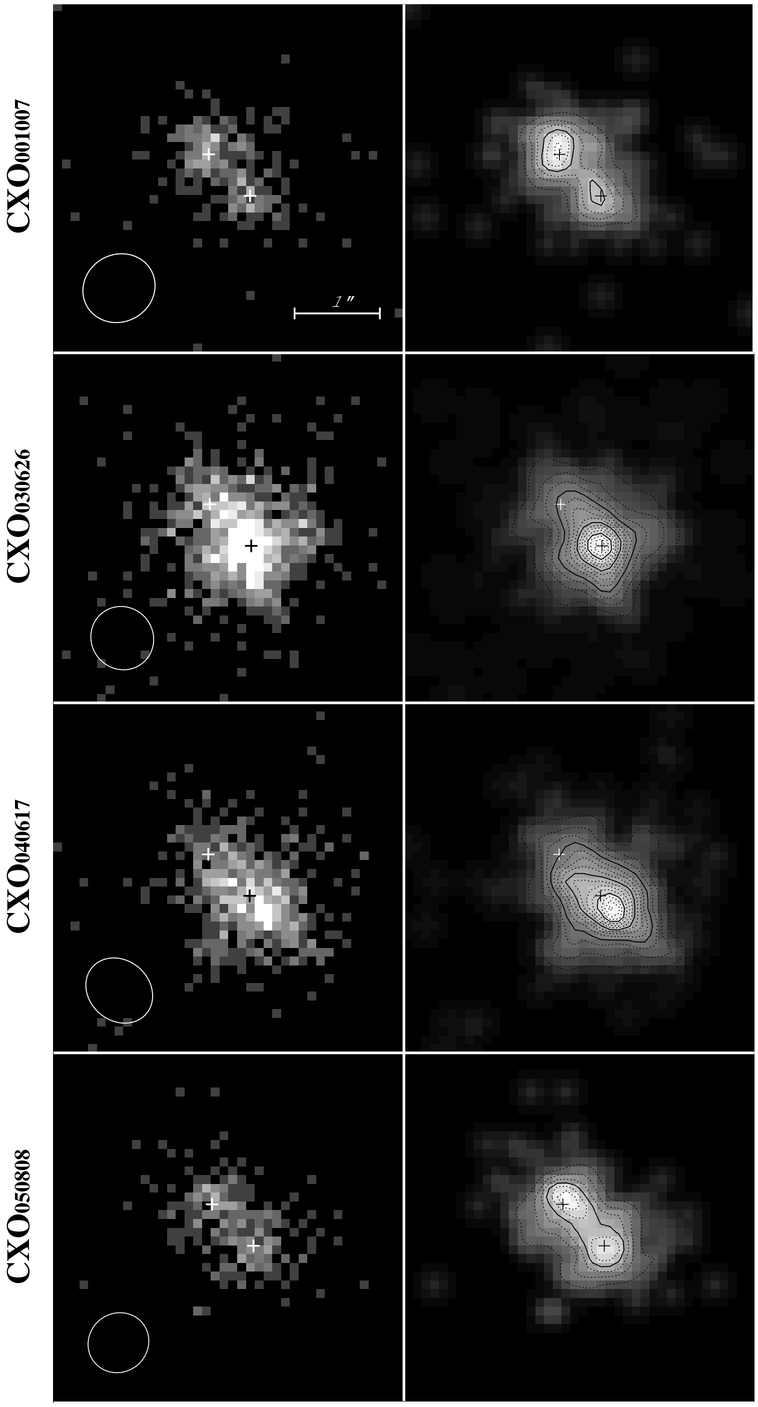

Fig. 1.— Magnified images of IRS 5 (raw: *left*, smoothed: *right*), sequentially in time from above. The gray scales are shown in a linear scale for all figures (but saturated above 10 cnts for the left panels). Crosses show X-ray source positions determined from our analysis. Circles at the bottom left of the left panels show the half of the peak intensity of the PSF. Raw image bins are 0.″123 pixel^{-1}. Gray scales and contours in the right panels are normalized by the effective area and exposure time in CXO$_{050808}$.

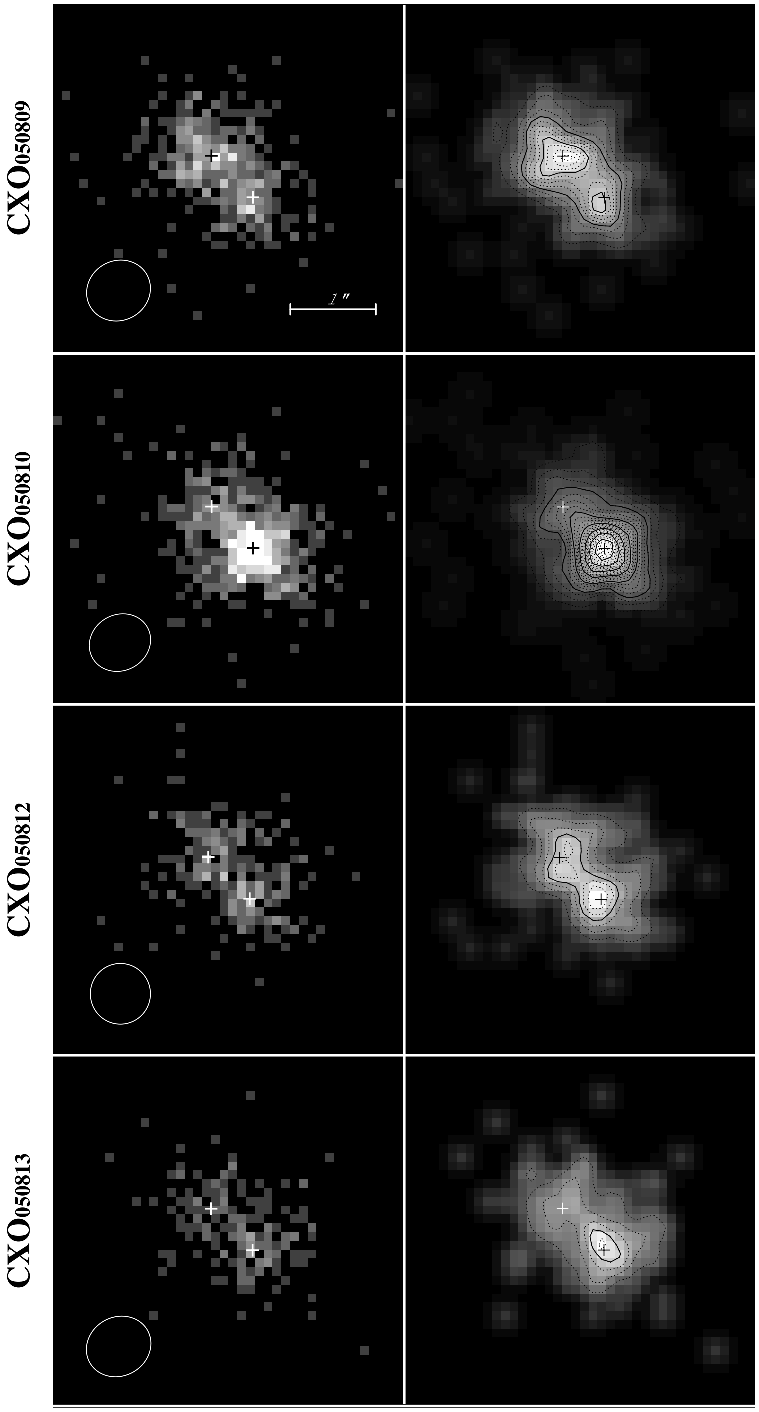

Fig. 1. — Continued.

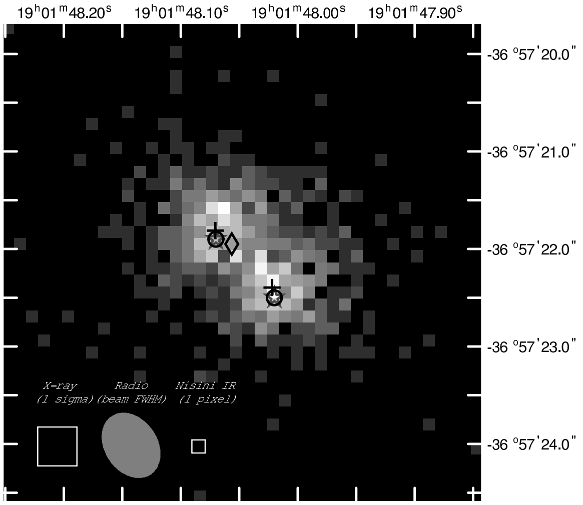

Fig. 2.— Composite of images in CXO$_{001007}$, CXO$_{050808}$, CXO$_{050812}$ and CXO$_{050813}$, when both of IRS 5a and IRS 5b were in the quiescent phase. Markers — cross: X-rays, circle: cm radio (Choi et al. 2008), diamond: 2MASS, star: infrared source positions in Nisini et al. (2005), shifted to match for the cm radio source positions. Error ranges of the X-ray source positions from the 2MASS frame (200 mas), radio beam size (Choi et al. 2008) and IR image pixel size (Nisini et al. 2005) are shown at the bottom left.

IRS 13 and HBC 667 (K ~7.0–10.5^m) have possible position inaccuracy of up to 100 mas RMS, except for the brightest source R CrA (K =2.9^m), which had a slightly larger position uncertainty of 160 mas (RMS)[5]. The uncertainty of the mean position of all the sources is ~50 mas. Combined with the cluster proper motion noted above, we can determine the absolute source position better than ~200 mas for these sources. Table 1 lists the shifts of the X-ray sky coordinate frame from the original X-ray data. Earlier observations in 2000−2003 needed relatively large shifts (~0.3−1″), while observations in 2005 needed almost negligible shifts ($\lesssim$0.2″). Table 1 also lists the standard offset deviation of the X-ray source positions from the 2MASS source positions. The result suggests that X-ray source positions in all the *Chandra* observations were determined at $\lesssim$200 mas from the 2MASS frame, and hence $\lesssim$400 mas in the absolute coordinate frame.

3.2. Image Analysis

Figure 1 shows X-ray images of IRS 5 between 1−8 keV after the absolute position correction. They were binned with 0.″123 pixel^{-1} to resolve sources having sub-arcsecond separation. In all the images, X-ray emission was clearly elongated toward the NE-SW direction. We checked in two ways if this structure is real. First, we created simulations of point spread functions (PSF) at the location of IRS 5 with `ChaRT` (Carter et al. 2003) and `MARX`[6] version 4.2.1, assuming a spectrum $N_{\rm H}$ =4.5×10^{22} cm^{-2}, kT =3 keV and Z =0.3 solar, (based on our preliminary fits of the IRS 5 spectra using the standard method). Second, we made images of IRS 1 with a similar off-axis angle to IRS 5 to determine if the SER method might introduce asymmetries in the PSF. We found no such extension from either of the half maximum PSF circles (Figure 1) nor the IRS 1 images. We conclude that the deduced elongation of the X-ray image of IRS 5 is real.

In CXO$_{030626}$, CXO$_{040617}$ and CXO$_{050810}$ the south-west part of the elongation was remarkably bright, while in CXO$_{050809}$ the north-east part looked slightly brighter than the south-west part. In the other observations, we recognized apparently two peaks with similar intensities. We re-ran the `wavdetect` source detection tool for these high resolution images and detected the south-west source in all observations, and detected the north-east source in CXO$_{001007}$, CXO$_{050808}$, CXO$_{050809}$ and CXO$_{050812}$. The north-east peak was not detected when the south-west peak was very bright or images lacked sufficient exposure. Both peaks were located at, on average, (α_{2000}, δ_{2000}) = ($19^h1^m48.^s07$, $-36°57'21.''8$) designated using the *Chandra* naming convention as CXOU J190148.1-365722 and (α_{2000}, δ_{2000}) = ($19^h1^m48.^s02$, $-36°57'22.''4$) as CXOU J190148.0-365722 and the positions of the individual detections differed by 0.″09 for the former and 0.″075 for the latter in RMS. These sources are separated by only ~0.″8±0.″12 (1σ), corresponding to a ~140 AU projected separation at $d = 170$ pc.

---

[5] http://www.ipac.caltech.edu/2mass/releases/allsky/doc/

[6] http://space.mit.edu/CXC/MARX/

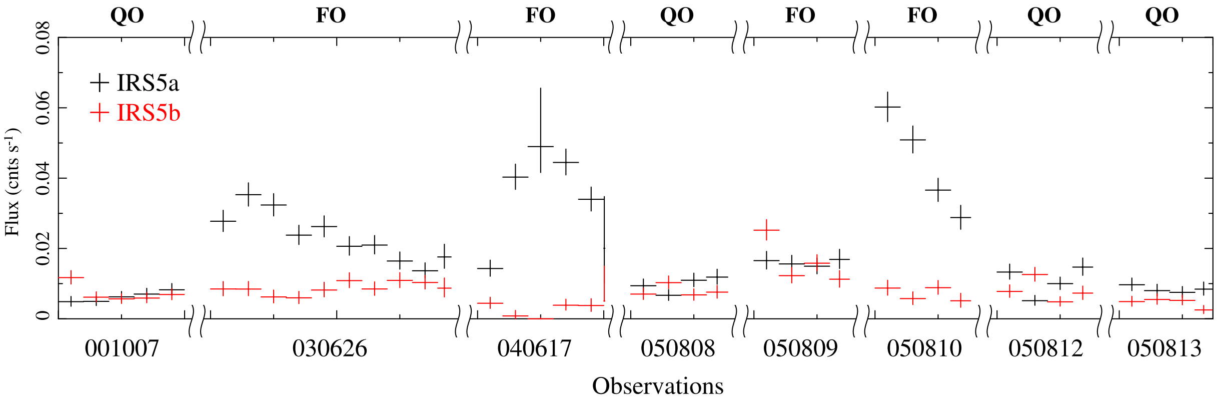

Fig. 3.— Light curves between 1−8 keV (*top*) of IRS 5a (*black*) and IRS 5b (*red*). Each bin has 4 ksec and tic marks on the horizontal axis are shown by 10 ksec from the beginning of each observation. The error bars show 1σ confidence range. In CXO$_{030626}$, CXO$_{040617}$, CXO$_{050810}$, and CXO$_{050813}$, IRS 5b emitted X-rays comparable to the other observations, but `wavdetect` did not detect it. This is probably because enhanced X-ray emission from IRS 5a contaminated strongly at the IRS 5b position, and thus increased the apparent background level (see §3.3). Labels at the top depict observations which showed significant X-ray variations in either of IRS 5a nor IRS 5b (FO: Flare Observation) or in neither of them (QO: Quiescent Observation).

A composite image of CXO$_{001007}$, CXO$_{050808}$, CXO$_{050812}$ and CXO$_{050813}$ clearly showed two peaks at the north-east and south-west sides (Figure 2). These X-ray peaks have corresponding cm radio counterparts within $\sim$0.″1 for each (Choi et al. 2008). They have offsets from the infrared sources IRS 5a and IRS 5b of $\sim$1″ according to their absolute coordinates in the H and K band maps in Figure 1 of Nisini et al. (2005). The 2MASS survey with an absolute astrometric accuracy of $\sim$100 mas detected an infrared source very close to the north-east X-ray source though it did not resolve the two infrared sources probably due to the limited spatial resolution of the CCD (2″). Moreover, the two X-ray sources and the IR sources in Nisini et al. (2005) have similar position angle and separation, and therefore match their positions well by shifting the IR image frame (see Figure 2). We therefore identified the south-west X-ray source (CXOU J190148.0-365722) as IRS 5a and the north-east source (CXOU J190148.1-365722) as IRS 5b.

3.3. Timing and Spectral Analysis with 2-Dimensional Image Fits

Because the X-ray emission from IRS 5a and IRS 5b is strongly blended, the standard method to generate light curves and spectra — counting photons within user defined source and background regions — cannot be used straightforwardly. Therefore we utilized the 2-dimensional image fitting method in which we generated multiple images from each observation in restricted time and energy ranges and fit each 2-dimensionally by the combined individual model PSF images for IRS 5a and IRS 5b. We created images with a size of 80 pixel × 80 pixel binned by 0.″123 pixel^{-1}. For the model images, we used the `ptsrc2d` function in the CIAO package, assuming two point source components at the position of the X-ray sources, and used the `sherpa` tool to carry out the fitting procedure (We should note that a part of the X-ray emission may come from different and/or extended regions.) We did not include background in the model images, since the background is negligibly small ($\sim 3\times10^{-4}$ cnts / (1 pixel=0.″123)^2 / 10 ksec). The `ptsrc2d` function loads an image as a template model PSF. Using these model PSFs, we generated photon events at the position of IRS 5 using both `ChaRT` (Carter et al. 2003) and `MARX`. For the light curve analysis, we assumed a PSF to have the typical spectrum of IRS 5 based on our preliminary analysis using the standard method, i.e. $N_{\rm H}$ $=4.5\times10^{22}$ cm^{-2}, kT =3 keV and 0.3 solar elemen-

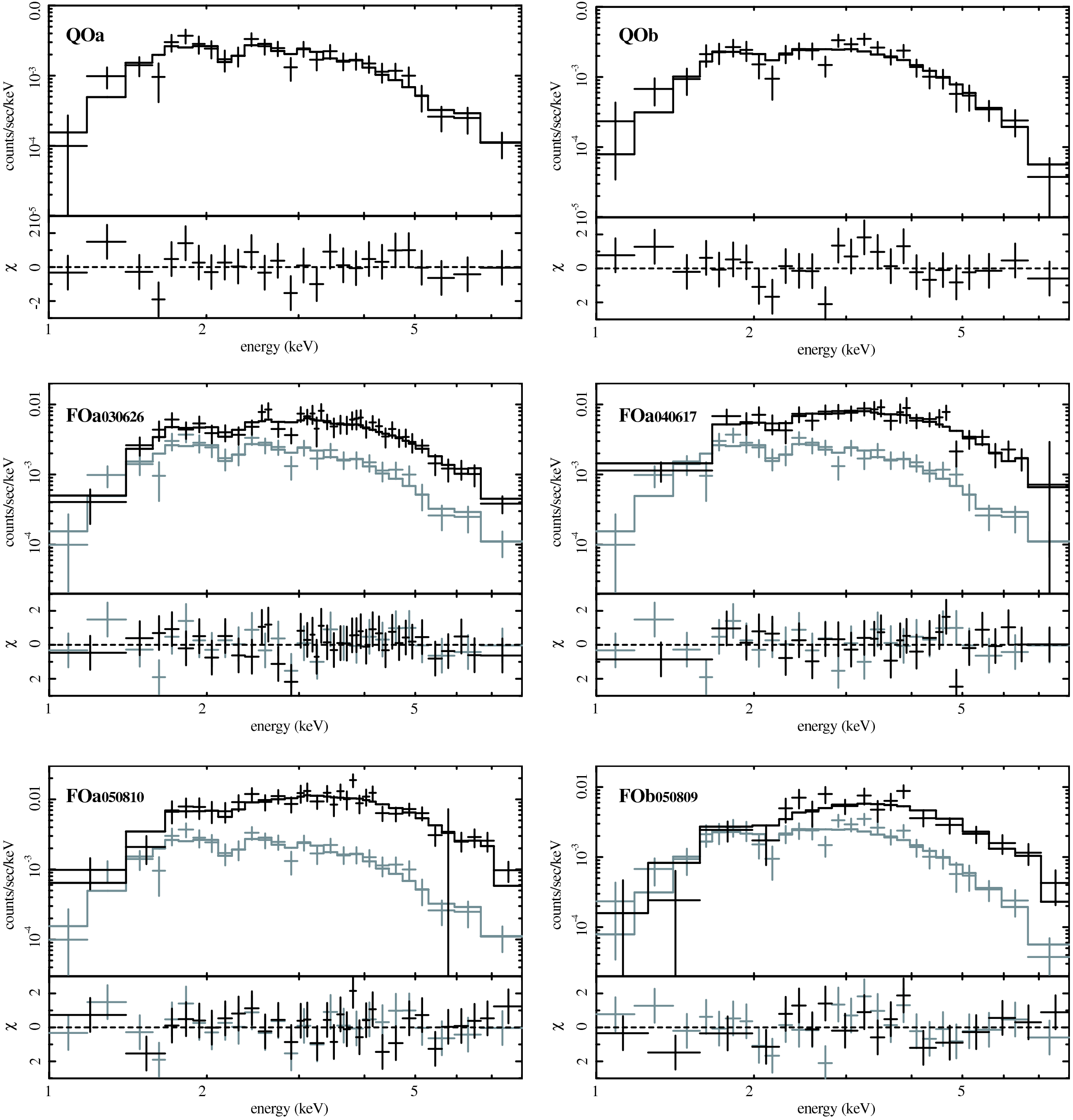

Fig. 4.— Quiescent spectra of IRS 5a (*top left*) and IRS 5b (*top right*) and flare spectra of IRS 5a in CXO$_{030626}$ (*middle left*), CXO$_{040617}$ (*middle right*), CXO$_{050808}$ (*bottom left*) and of IRS 5b in CXO$_{050809}$ (*bottom right*), overlaid on the quiescent spectra (grey).

Table 2
Spectral Fits

Source	Spectrum	Photon (counts)	Model	kT (keV)	$N_{\rm H}$ (10^{22} cm^{-2})	χ^2/d.o.f (d.o.f.)	$L_{\rm X}$ (10^{30} erg s^{-1})
IRS5a	QOa	490.6	1T	2.2 (1.7−3.2)	3.7 (3.0−4.5)	0.78 (24)	1.5
	FOa$_{030626}$	771.9	1T (+QOa)	5.4 (>2.8)	4.7 (3.3−6.8)	0.58 (64)	2.5
	FOa$_{040617}$	554.1	1T (+QOa)	5.4 (>2.8)	5.1 (3.7−6.8)	0.67 (52)	4.4
	FOa$_{050810}$	597.5	1T (+QOa)	6.6 (>3.4)	5.1 (4.1−6.5)	0.69 (57)	6.2
IRS5b	QOb	493.0	1T	2.0 (1.5−2.5)	4.5 (3.7−5.8)	0.92 (24)	1.9
	FOb$_{050809}$	292.0	1T (+QOb)	4.4 (>1.4)	7.8 (5.1−14.4)	0.89 (43)	3.3

Note.—QO: Quiescent Observation. FO: Flare Observation. Photon: net photon counts between 1−8 keV. Absorption corrected $L_{\rm X}$ between 0.5−10 keV, assuming the distance of 170 pc. Values in parentheses denote formal 90% confidence limits, and do not include any systematic errors produced by our 2-dimensional fitting procedure. The elemental abundance was fixed at 0.3 solar value.

tal abundance. In both the timing and spectral analyses, we generated PSF images in the same energy band as the observed images using large numbers of photon events to minimize statistical fluctuations. In the `sherpa` fits, we fixed the centroids of two point source components at the X-ray source positions of IRS 5a and IRS 5b and only allowed their normalization parameters to vary. We used the Cash statistic appropriate for Poisson-limited data and used the Powell method to find the best-fit values. We derived upper and lower boundaries of the 1σ confidence range using the `projection` function.

Figure 3 shows individual light curves of IRS 5a and IRS 5b in 4 ksec bins in the energy range 1−8 keV. We normalized the individual lightcurves to the 3 keV effective area at the position of IRS 5a, resulting in small correction factors ($\lesssim$1 %). Their flux variations look to be uncorrelated, suggesting no significant interference with each other in our 2-dimensional fits. To further check the consistency of the image fitting results, we summed the individual light curves of IRS 5a and IRS 5b and compared them to a light curve extracted from the entire IRS 5 complex, including photon counts within a $3''$ radius circle centered on between IRS5a and IRS5b, which include ∼90−93% of photons from both IRS 5a and IRS 5b. We found that the standard method obtained 93−98% of the photon counts we derived by combining the individual IRS 5a and IRS 5b photons. We had similar results for the split energy bands between 1−3.5 keV and 3.5−8 keV, which we used for a hardness ratio analysis described in the next paragraph. This suggests that our image fitting method produces a result that is consistent with the standard method within $\lesssim$10% discrepancy.

In CXO$_{030626}$, CXO$_{040617}$, and CXO$_{050810}$, IRS 5a showed significant time variations, reminiscent of stellar X-ray flares. The fast rise (∼4 ksec in CXO$_{040617}$) and slow decay (a half decay time of 15−30 ksec) time scales based on visual inspection were similar to those of relatively strong X-ray flares from YSOs. The flux level did not change remarkably during the other observations ($\lesssim$50%). IRS 5b was quite stable in almost all the available observations. The non-detection of IRS 5b with `wavdetect` in 4 observations would be therefore caused by increased contamination from IRS 5a by flares, or from limited photon statistics. IRS 5b showed a small flux enhancement by a factor of 2 in CXO$_{050809}$, and an apparent decrease at the middle of CXO$_{040617}$, but this decline could be an artifact produced by strong contamination from the IRS 5a flare in this observation along with a possible offset of the southwest emission peak from IRS 5a. We split the energy band into two at 3.5 keV, which is near the median of the photon distribution against energy in a spectrum, and measured the hardness ratio (HR) of each observation, which we have defined as $HR = (H - S)/(H + S)$, where the H and S are count rates of the 3.5−8 keV and 1−3.5 keV bands, respectively. The average HRs of both IRS 5a and IRS 5b in CXO$_{001007}$, CXO$_{050808}$, CXO$_{050812}$ and CXO$_{050813}$, when neither showed significant variations (and which we refer to as the "quiescent observations"), were $HR \sim -0.32\pm0.15$, -0.29 ± 0.18 (1σ), respectively. The HRs were $\sim -0.02\pm0.09$ (1σ) during flares from IRS 5a (CXO$_{030626}$, CXO$_{040617}$, CXO$_{050810}$) and $\sim0.04\pm0.08$ (1σ) during a small flux enhancement of IRS 5b (CXO$_{050809}$). The HR was slightly higher in the flare than during the quiescent observations.

We generated individual spectra of IRS 5a and IRS 5b in key phases and analyzed them with `xspec` version 11. One technical issue was that `xspec` requires integer photon counts, while the `ptsrc2d` function outputs the normalization values (i.e. photon counts) in floating point. Thus, to avoid any round off error, we multiplied photon counts and exposure time by 1000 when creating spectral files. The `xspec` format also assumes a single error value for each spectral bin, while the `projection` function outputs upper and lower error ranges. We therefore used the larger value output from `projection` as the `xspec` error for each spectral bin. Since we set most of the spectral bins to have $\gtrsim$15 photons the upper and lower error ranges typically have less than ~10% differences. We generated response matrices and auxiliary files corresponding to the spectral files using `mkacisrmf` and `mkarf` in the CIAO package.

Since no quiescent observation had enough photon statistics to generate a spectrum with sufficient signal-to-noise, we combined images of these observations in each spectral bin. We combined their PSF images and spectral responses as well for our 2-dimensional image fits and spectral model fits. The result is shown in Figure 4. The quiescent spectra of IRS 5a and IRS 5b were almost identical with significant emission up to ~8 keV and a cut-off due to absorption at ~1.5 keV. We modeled both spectra using an absorbed optically thin, 1-temperature (1T) plasma model (WABS, Morrison & McCammon 1983; APEC[7], Table 2). The best-fit models had $N_{\rm H} \sim 4\times10^{22}$ cm^{-2} and $kT \sim 2$ keV for both sources. The absorption corrected log $L_{\rm X}$ was 30.2−3 (0.5−10 keV).

We compared the IRS 5a spectra during flaring states (CXO$_{030626}$, CXO$_{040617}$ and CXO$_{050810}$) to its quiescent spectrum (Figure 4). All flare spectra showed stronger emission in the 1−8 keV energy band than the quiescent spectrum. We fit the flare spectra by an absorbed 1T plasma model plus the best-fit model of the quiescent IRS 5a spectrum, assuming that a new plasma component appeared during the flares. The best fit to the flare spectra seems to have higher kT (~5−7 keV) than the quiescent spectrum but similar $N_{\rm H}$ ($\sim5\times10^{22}$ cm^{-2}). However, IRS 5b showed similar increase in hard band flux in CXO$_{050809}$ compared to the quiescent phase, while the flux below ~2 keV was apparently unchanged (Figure 4). The best fit, assuming an absorbed 1T model plus the best-fit model of the quiescent IRS 5b spectrum showed significantly larger $N_{\rm H} \sim 7.8^{+4.2}_{-1.6}\times10^{22}$ cm^{-2} (1σ), which does not overlap with $N_{\rm H}$ in the quiescent spectrum ($4.5^{+0.4}_{-0.5}\times10^{22}$ cm^{-2}, 1σ). The best-fit model also showed slightly higher $kT \sim 4$ keV than the quiescent spectrum. None of these spectra had enough photon statistics to show the Fe line profile, which appeared in some flare spectra of the entire IRS 5a complex.

The values of $N_{\rm H}$ and kT for IRS 5a and IRS 5b are similar in all the observations and are consistent with the values in Forbrich et al. (2006), which were derived from the combined spectra of IRS 5a and IRS 5b. The kT and $L_{\rm X}$ values are typical of those from TTSs and Class I protostars, while the derived $N_{\rm H}$ is typical of Class I protostars (e.g., Imanishi et al. 2001).

4. Discussion

We still have a discrepancy between the positions of the near-infrared sources in Nisini et al. (2005) and the sources detected by 2MASS, VLA and *Chandra*. IRS 5a was a factor of two brighter than IRS 5b in Nisini et al. (2005), while the 2MASS source, whose position should be biased toward the brighter source (IRS 5a), was instead closer to IRS 5b (see §3.2). The 2MASS source is unlikely to be mis-positioned due to surrounding contamination since both IRS 5a and IRS 5b are sufficiently bright in the images shown in Figure 1 of Nisini et al. (2005). IRS 5a or IRS 5b might have experienced an increase in its near-infrared flux during the observations in Nisini et al. (2005) or during the 2MASS observations. We should note that IRS 5 only showed variation of less than ±0.03mag during monitoring observations in 2005 (see Figure 6 of Forbrich et al. 2007).

It is possible that the X-ray sources we have

---

[7] http://cxc.harvard.edu/atomdb/

Table 3

Young Binary System with <200 AU Projected Separation Resolved in X-rays

Object	System	Separation		Distance	Age	Reference
		sky (arcsec)	projection (AU)	(pc)	(Myr)	
TWA 5	M3Ve (TTS) + M8.5−9 (BD)	2	110	55	12	Tsuboi et al. (2003)
HD 100453	A9Ve + M4−M4.5 (TTS)	1.06	114	120	20	Collins et al. in prep.
HD 98800	K5Ve (TTS) + ?	0.8	48	38	5−10	Kastner et al. (2004)
R CrA IRS 5	K5-K7V (Class I) + ?	0.8	140	170	0.3−0.5 or 1.3[a]	this result

Note.—TTS: T-Tauri Star, BD: Brown Dwarf.

[a] Values of IRS 5a from Nisini et al. (2005).

identified with either IRS 5a or IRS 5b could be a background red giant star or an active galactic nucleus, though this is unlikely. However, X-ray emission from red giant stars are not usually as bright as, nor as hot as, emission from IRS 5a or IRS 5b (Pizzolato et al. 2000). Though some AGNs are observed with fluxes similar to those from IRS 5a or IRS 5b, the X-ray spectra are generally harder (spectral photon index $\Gamma \lesssim 2$, ex. Ueda et al. 1998) than those observed for either IRS 5a or IRS 5b ($\Gamma \sim 3.5$ assuming an absorbed power-law model). On the other hand, Pontoppidan et al. (2003) showed CO ice absorption lines of IRS 5a and IRS 5b have similar systemic velocities to the other YSOs in the R CrA cloud (~ -20 km s^{-1}) though this feature can be produced by an absorber physically unrelated to the infrared sources. The X-ray spectra are typical X-ray emission from Class I protostars. These results suggest that IRS 5a and IRS 5b form a protostar binary system within the R CrA cloud.

Table 3 shows binary systems with projected separations less than 200AU that have been spatially resolved in X-rays. According to this table, IRS 5 is the first X-ray binary system believed to be comprised of Class I protostars[8] and is a factor of $\gtrsim$10 younger than the other systems. Binary systems with linear separations of less than 140 AU have very little disk mass, perhaps because of the gravitational influence of the binary companion (Beckwith et al. 1990). The IRS 5 binary separation is near this boundary and the separation may be smaller if the distance is $d \sim$130 pc. The separation is so large that the binary stars would not have direct interaction by magnetic field, for example (see Uchida & Sakurai 1985 as an example of the system with magnetic interaction), but they may have an influence as discussed by Beckwith et al. (1990). IRS 5 may be an important example of the influence on X-ray activity of binary interaction in a very early phase.

The column densities of IRS 5a and IRS 5b derived from their X-ray spectra ($\sim 4\times10^{22}$ cm^{-2}) were typical of Class I protostars (c.f. Imanishi et al. 2001). These values of $N_{\rm H}$ were a factor of 2 smaller than the $N_{\rm H}$ value estimated from $A_{\rm V}$ for IRS 5a ($\sim$45 mag), assuming an empirical $N_{\rm H}-A_{\rm V}$ relation appropriate to the ρ Oph cloud (Imanishi et al. 2001). This result was consistent with X-ray absorption measurements of IRS1, 2 and 5 (Forbrich et al. 2006) and qualitatively consistent with a small $N_{\rm H}/{\rm A_J}$ ratio of the R CrA cloud (Vuong et al. 2003). The moderate $N_{\rm H}$ may not suggest the edge-on geometry discussed by Nisini et al. (2005) since X-rays from the stellar core would suffer stronger extinction in the edge-on disk than infrared emission from the stellar core and inner disk.

The kT and $L_{\rm X}$ values of the quiescent spectra of both IRS 5a and IRS 5b are typical of Class I protostars and TTSs (Imanishi et al. 2001). Assuming the mass of IRS 5a between 0.4−0.9 $M_{\odot}$ (Nisini et al. 2005), the $L_{\rm X} \sim 10^{30.2}$ erg s^{-1} corresponds to a $\sim$1 M-year-old pre-main sequence star based on the $L_{\rm X}$-age relation of young stars in the Orion nebula though the relation has a large scatter (Preibisch & Feigelson 2005). The kTs during the flares of IRS 5a are typical of YSOs (e.g.,

---

[8] Although the infrared spectral slope, which defines the YSO classification, has not been measured for IRS 5b, we think this star is a Class I protostar based on its high absorption in X-rays.

Imanishi et al. 2001; Wolk et al. 2005).

IRS 5a exhibited 3 prominent flares during the 8 *Chandra* observations. Since the observations ended at the middle of these flares, we only know lower limits to the flare durations ($\gtrsim$37.6, 19.9 and 15.0 ksec) and total flare energies ($\gtrsim$9.2, 8.7 and 9.3 $\times10^{34}$ ergs), respectively. These flares were similar in brightness to that of the brightest flares from classical TTSs and weak-line TTSs observed in the XEST project (Fig. 9 of Stelzer et al. 2007). Curiously, we did not see any flare-like event from IRS 5a fainter than those flares though such flares would have been detectable. IRS 5a had 3 flares during the 152 ksec exposure, that is, one flare per $\sim$50 ksec. This is more than an order of magnitude more frequent than the average of the XEST (1 flare in 770 ksec for flares with the flare energies above 10^{35} ergs, Stelzer et al. 2007) and COUP (1 flare in 650 ksec, Wolk et al. 2005), though we did not consider possible detections of flares that start outside the observing window. IRS 5 showed remarkable variation in the other *XMM-Newton* observations too (Forbrich et al. 2006), for which either of IRS 5a or IRS 5b would be responsible. IRS 5a seems to be an actively flaring source, though the accretion rate was measured to be low (Nisini et al. 2005).

IRS 5b did not show apparent variation during the *Chandra* observations except for a flux enhancement in CXO_{050809}. The column density of IRS 5b during the flux enhancement increased by a factor of $\sim$2 from the quiescent phase. Such variable X-ray emission in CXO_{050809} might have been produced from a plasma on or around the stellar surface that appeared behind the circumstellar disk, or perhaps IRS 5b may have another deeply embedded companion.

Except for the flare activity, X-ray properties of IRS 5a and IRS 5b are strikingly similar. This may strengthen a general assumption that stars in a similar mass range experience similar evolution of their quiescent X-ray spectra. This result also raises a caution in measurements of the L_{X} function of YSOs — L_{X} can be significantly overestimated if a YSO has an unresolved companion.

5. Conclusion

We spatially resolved X-ray emission from each component of the infrared double system IRS 5 in the R CrA molecular cloud with a $0.''8$ projected separation in 8 *Chandra* observations. Their X-ray brightnesses and spectra suggest that they are a Class I protostar binary system. Separations of binary YSOs are typically less than $\sim10''$ in nearby star forming regions. *Chandra* enabled study of X-ray properties of such young binary systems for the first time.

We derived light curves and spectra of these objects using a 2-dimensional image fitting method. During the 8 *Chandra* observations, the southern source IRS 5a showed three X-ray flares lasting more than 15 ksec and with flare energies of $\gtrsim10^{35}$ ergs. These flares were relatively powerful compared to flares from classical TTSs and weak-line TTSs. The flare frequency (1 flare per $\sim$50 ksec) was higher than flares from PMSs in the Taurus and Orion cloud. IRS 5a might be in an active phase, or may have a different mechanism which drives its X-ray flares. IRS 5b, on the contrary, did not show strong variation through the observations, except for a flux increase by a factor of two in 2007 Aug. 9 accompanied by an apparent N_{H} increase.

Though IRS 5a and IRS 5b had clear differences in their X-ray variability, their quiescent X-ray spectra were almost identical. This may suggest that both stars have gone through a similar evolutionary phase in X-ray activity. Detailed infrared spectroscopy of IRS 5b is crucial to determine its stellar parameters and to understand nature of the IRS 5 system. Measurement of proper and radial motions of both IRS 5a and IRS 5b would be also important to understand whether they are a gravitationally bound system.

This work is performed while K.H. was supported by the NASA Astrobiology Program under CAN 03-OSS-02. This publication makes use of data products from the Two Micron All Sky Survey, which is a joint project of the University of Massachusetts and the Infrared Processing and Analysis Center/California Institute of Technology, funded by the National Aeronautics and Space Administration and the National Science Foundation. This research has made use of data obtained from the High Energy Astrophysics Science Archive Research Center (HEASARC), provided by NASA's Goddard Space Flight Center.

Facilities: CXO(ACIS-I)

REFERENCES

Beckwith, S. V. W., Sargent, A. I., Chini, R. S., & Güsten, R. 1990, AJ, 99, 924

Carkner, L., Mamajek, E., Feigelson, E., Neuhäuser, R., Wichmann, R., & Krautter, J. 1997, ApJ, 490, 735

Carter, C., Karovska, M., Jerius, D., Glotfelty, K., & Beikman, S. 2003, in Astronomical Society of the Pacific Conference Series, Vol. 295, Astronomical Data Analysis Software and Systems XII, ed. H. E. Payne, R. I. Jedrzejewski, & R. N. Hook, 477

Casey, B. W., Mathieu, R. D., Vaz, L. P. R., Andersen, J., & Suntzeff, N. B. 1998, AJ, 115, 1617

Chabrier, G., & Küker, M. 2006, A&A, 446, 1027

Chen, W. P., & Graham, J. A. 1993, ApJ, 409, 319

Choi, M., Hamaguchi, K., Lee, J.-E., & Tatematsu, K. 2008, ApJ, accepted

Dobler, W., Stix, M., & Brandenburg, A. 2006, ApJ, 638, 336

Duchêne, G., Delgado-Donate, E., Haisch, Jr., K. E., Loinard, L., & Rodríguez, L. F. 2007, in Protostars and Planets V, ed. B. Reipurth, D. Jewitt, & K. Keil, 379–394

Feigelson, E. D., Carkner, L., & Wilking, B. A. 1998, ApJ, 494, L215

Forbrich, J., & Preibisch, T. 2007, A&A, 475, 959

Forbrich, J., Preibisch, T., & Menten, K. M. 2006, A&A, 446, 155

Forbrich, J., et al. 2007, A&A, 464, 1003

Hamaguchi, K., Corcoran, M. F., Petre, R., White, N. E., Stelzer, B., Nedachi, K., Kobayashi, N., & Tokunaga, A. T. 2005, ApJ, 623, 291

Imanishi, K., Koyama, K., & Tsuboi, Y. 2001, ApJ, 557, 747

Kastner, J. H., Huenemoerder, D. P., Schulz, N. S., Canizares, C. R., Li, J., & Weintraub, D. A. 2004, ApJ, 605, L49

Knude, J., & Hϕg, E. 1998, A&A, 338, 897

Koyama, K., Hamaguchi, K., Ueno, S., Kobayashi, N., & Feigelson, E. D. 1996, PASJ, 48, L87

Li, J., Kastner, J. H., Prigozhin, G. Y., & Schulz, N. S. 2003, ApJ, 590, 586

Li, J., Kastner, J. H., Prigozhin, G. Y., Schulz, N. S., Feigelson, E. D., & Getman, K. V. 2004, ApJ, 610, 1204

Marraco, H. G., & Rydgren, A. E. 1981, AJ, 86, 62

Monin, J.-L., Clarke, C. J., Prato, L., & McCabe, C. 2007, in Protostars and Planets V, ed. B. Reipurth, D. Jewitt, & K. Keil, 395–409

Morrison, R., & McCammon, D. 1983, ApJ, 270, 119

Neuhäuser, R., & Preibisch, T. 1997, A&A, 322, L37

Nisini, B., Antoniucci, S., Giannini, T., & Lorenzetti, D. 2005, A&A, 429, 543

Perryman, M. A. C., & ESA, eds. 1997, ESA Special Publication, Vol. 1200, The HIPPARCOS and TYCHO catalogues. Astrometric and photometric star catalogues derived from the ESA HIPPARCOS Space Astrometry Mission

Pizzolato, N., Maggio, A., & Sciortino, S. 2000, A&A, 361, 614

Pontoppidan, K. M., Fraser, H. J., Dartois, E., Thi, W.-F., van Dishoeck, E. F., Boogert, A. C. A., d'Hendecourt, L., Tielens, A. G. G. M., & Bisschop, S. E. 2003, A&A, 408, 981

Preibisch, T., & Feigelson, E. D. 2005, ApJS, 160, 390

Stelzer, B., Flaccomio, E., Briggs, K., Micela, G., Scelsi, L., Audard, M., Pillitteri, I., & Güdel, M. 2007, A&A, 468, 463

Suters, M., Stewart, R. T., Brown, A., & Zealey, W. 1996, AJ, 111, 320

Taylor, K. N. R., & Storey, J. W. V. 1984, MNRAS, 209, 5P

Tsuboi, Y., Maeda, Y., Feigelson, E. D., Garmire, G. P., Chartas, G., Mori, K., & Pravdo, S. H. 2003, ApJ, 587, L51

Tsunemi, H., Mori, K., Miyata, E., Baluta, C., Burrows, D. N., Garmire, G. P., & Chartas, G. 2001, ApJ, 554, 496

Uchida, Y., & Sakurai, T. 1985, in IAU Symposium, Vol. 107, Unstable Current Systems and Plasma Instabilities in Astrophysics, ed. V. Dogiel & V. A. Dogel', 281–285

Ueda, Y., Takahashi, T., Inoue, H., Tsuru, T., Sakano, M., Ishisaki, Y., Ogasaka, Y., Makishima, K., Yamada, T., & Ohta, K. 1998, Nature, 391, 866

Vuong, M. H., Montmerle, T., Grosso, N., Feigelson, E. D., Verstraete, L., & Ozawa, H. 2003, A&A, 408, 581

Wang, H., Mundt, R., Henning, T., & Apai, D. 2004, ApJ, 617, 1191

Weisskopf, M. C., Brinkman, B., Canizares, C., Garmire, G., Murray, S., & Van Speybroeck, L. P. 2002, PASP, 114, 1

Wilking, B. A., Greene, T. P., Lada, C. J., Meyer, M. R., & Young, E. T. 1992, ApJ, 397, 520

Wilking, B. A., Taylor, K. N. R., & Storey, J. W. V. 1986, AJ, 92, 103

Wolk, S. J., Harnden, Jr., F. R., Flaccomio, E., Micela, G., Favata, F., Shang, H., & Feigelson, E. D. 2005, ApJS, 160, 423

This 2-column preprint was prepared with the AAS LaTeX macros v5.2.